Article

Discovery Medicine 2026; 38(214): 3687–3698
https://doi.org/10.24976/Discov.Med.202638214.280

Calycosin Ameliorates Chronic Renal Failure Through the NCOA2/NF-κB/NLRP3 Signaling Pathway

Jiangen Yu[1], Wenzhen Yang[1], Xiaoyun Zhang[1], Subo Li[1], Hongzhen Ma[2], Lin Li[3,*]

[1]Department of Nephrology, The First People's Hospital of Xiaoshan District (Xiaoshan Affiliated Hospital of Wenzhou Medical University), 311200 Hangzhou, Zhejiang, China
[2]Department of Nephrology, The First Affiliated Hospital of Zhejiang Chinese Medical University (Zhejiang Provincial Hospital of Chinese Medicine), 310006 Hangzhou, Zhejiang, China
[3]Department of Hemodialysis Center, The First People's Hospital of Xiaoshan District (Xiaoshan Affiliated Hospital of Wenzhou Medical University), 311200 Hangzhou, Zhejiang, China
*Correspondence: 13506715625@163.com (Lin Li)
Submitted: 15 September 2026 Revised: 1 November 2026 Accepted: 4 November 2026 Published: 25 November 2026

Background: Chronic renal failure (CRF) represents a clinical syndrome characterized by severe renal dysfunction, with inflammation and fibrosis. Calycosin has demonstrated promising renoprotective effects; however, the molecular mechanisms underlying these protective effects have not been fully clarified. This study aimed to explore the protective effects of calycosin on CRF and clarify the role of the nuclear receptor coactivator 2 (NCOA2)/nuclear factor kappa B (NF-κB)/NLR family pyrin domain-containing protein 3 (NLRP3) signaling axis.

Methods: An adenine-induced CRF rat model was constructed, and rats received interventions with different doses of calycosin. Renal function was assessed by measuring serum creatinine (Scr), blood urea nitrogen (BUN), and uric acid (UA) levels. Hematoxylin and eosin (HE) staining and Masson's Trichrome staining were used to evaluate renal pathological alterations. The concentrations of inflammatory factors, including interleukin-1β (IL-1β), interleukin-6 (IL-6), and tumor necrosis factor-α (TNF-α), were measured using commercial enzyme-linked immunosorbent assay (ELISA) kits. The activation of NLRP3/NF-κB signaling and pyroptosis-related proteins was analyzed by Western blotting. Molecular docking analysis was performed to predict the favorable binding affinity between calycosin and NCOA2. Furthermore, NCOA2 overexpression experiments were performed to investigate its role in calycosin-mediated renoprotection.

Results: Calycosin intervention markedly alleviated renal pathological injury and improved renal function in CRF rats, accompanied by lowered serum Scr ($p < 0.001$) and BUN ($p < 0.01$), suppressed inflammatory cytokine production ($p < 0.001$), and downregulated NLRP3 expression ($p < 0.001$). Molecular docking analysis revealed a favorable interaction between calycosin and NCOA2, with a binding energy of –6.7 kcal/mol. NCOA2 overexpression partially reversed the inhibitory effects of calycosin on NLRP3 expression ($p < 0.001$) and inflammatory cytokine production ($p < 0.001$), and aggravated renal pathological injury ($p < 0.01$). Mechanistically, calycosin suppressed NF-κB p65 nuclear translocation, decreased NLRP3 expression, and inhibited pyroptosis-related molecular signaling ($p < 0.05$).

Conclusion: This study suggests that calycosin alleviates renal injury in the adenine-induced CRF rat model, and its renoprotective effect is associated with the NCOA2/NF-κB/NLRP3 signaling axis, thereby suppressing inflammatory responses and pyroptosis-related molecular mechanisms.

Keywords: chronic renal failure; calycosin; inflammation; pyroptosis; renal injury

Introduction

Chronic renal failure (CRF) is a clinical syndrome caused by progressive and irreversible damage of nephrons due to chronic bilateral renal lesions, characterized by impaired renal homeostatic regulation [1]. This disorder leads to significant metabolic disturbances and manifests with pathological alterations across multiple organ systems [2]. Clinically, renal replacement therapy serves as the mainstay intervention for CRF. Globally, an estimated 850 million people live with chronic kidney disease (CKD), and approximately 4 million patients with renal failure require renal replacement therapy [3]. With the exacerbation of the aging population structure, CRF resulting from progressive CKD has become a major global health issue. However, the long-term economic burden and increased cardiovascular risk associated with maintenance dialysis, together with the limited availability of kidney transplant sources, significantly diminish the practical effectiveness of renal replacement therapy [4].

Inflammation and fibrosis are two key processes that determine the progression of CRF. Due to the persistent in-

Copyright: © 2026 The Author(s). Published by Discovery Medicine. This is an open access article under the CC BY 4.0 license.
Note: *Discovery Medicine* stays neutral with regard to jurisdictional claims in published maps and institutional affiliations.

flammatory state, CRF patients experience excessive production of various inflammatory mediators in their kidneys [5]. Among various pattern recognition receptors, the NLR family pyrin domain-containing protein 3 (NLRP3) inflammasome has emerged as a key focus of research in nephrology. Aberrant activation of NLRP3 inflammasome activity plays a pivotal role in the pathogenesis and progression of chronic kidney disease [6]. A previous study showed that inhibiting the NLRP3 inflammasome can reduce blood pressure, serum creatinine (Scr), and blood urea nitrogen (BUN) levels, and improve glomerular filtration function, thereby alleviating kidney inflammation [7]. The activated NLRP3 inflammasome can mediate kidney injury in a diabetic nephropathy mouse model by inhibiting podocyte autophagy [8]. Thus, inhibiting NLRP3 inflammasome activation and its downstream signaling cascades may constitute a promising therapeutic strategy for chronic kidney disease.

In recent years, bioactive phytochemicals have garnered growing interest as promising therapeutic agents for kidney diseases due to their anti-inflammatory, antioxidant, and antifibrotic properties [9,10,11]. Calycosin, an isoflavonoid compound extracted from *Astragalus membranaceus*, has been reported to exert favorable protective effects against renal injury [12]. Calycosin alleviates renal fibrosis by reducing neutrophil extracellular trap (NET) formation through the Toll-like receptor 4 (TLR4)/nuclear factor kappa-B (NF-κB) signaling pathway [13]. In addition, calycosin alleviates endoplasmic reticulum stress-induced injury in human glomerular endothelial cells through the suppression of reactive oxygen species (ROS) production [14]. These findings suggest that calycosin may exert renoprotective effects through the regulation of inflammatory and oxidative stress-related pathways.

To further explore the potential molecular targets of calycosin, active compound screening was performed using the HERB database and the Traditional Chinese Medicine Systems Pharmacology Database and Analysis Platform (TCMSP). Nuclear receptor coactivator 2 (NCOA2) was predicted to be a potential target of calycosin. A previous study has shown that in a lipopolysaccharide (LPS)-induced acute kidney injury mouse model, NF-κB subunits p50 and p65 can interact with lysine acetyltransferase 2B (KAT2B) and NCOA2 to form a transcriptional regulatory complex [15]. This NCOA2-KAT2B-NF-κB complex binds to the promoter regions of NF-κB target genes and facilitates their transcriptional activation, thereby amplifying inflammatory responses. Based on these reports, we hypothesized that calycosin may attenuate renal inflammation through a potential interaction with NCOA2 and by disrupting NCOA2-mediated NF-κB activation, ultimately suppressing the expression of downstream inflammatory mediators. Therefore, an adenine-induced CRF rat model was constructed to assess whether calycosin could attenuate renal injury progression and alleviate renal inflammation. Furthermore, the involvement of the calycosin/NCOA2/NF-κB axis in regulating inflammatory responses during CRF progression was investigated to elucidate the underlying molecular mechanisms.

Materials and Methods

The Establishment of a Rat Model of CRF and Grouping

A total of 66 male Sprague-Dawley (SD) rats aged 6-8 weeks, weighing 200–250 g, were obtained from Hangzhou Medical College (China). All animals underwent a 3-day environmental acclimation period. The lighting schedule was set from 7:00 AM (lights on) to 7:00 PM (lights off) to establish a normal circadian rhythm.

First, 30 SD rats were randomly allocated into five experimental groups using a random number table method (n = 6 per group): Control (Con) group, CRF model (Mod) group, Mod+calycosin-Low concentration (cal-L), Mod+calycosin-Middle concentration (cal-M) and Mod+calycosin-High concentration (cal-H). Rats in the Con group received standard food and water *ad libitum*. A 2.5% adenine solution was prepared by dissolving adenine (pure: ≥99%, A8626, Merck, Sigma-Aldrich, St. Louis, MO, USA) in normal saline (100 mL, ST341, Beyotime, Shanghai, China) [16]. Rat in the Mod group received adenine administration at a dosage of 200 mg/kg through daily gavage for 28 consecutive days. For calycosin intervention, following 14 days of adenine administration, rats in the Mod+cal-L, Mod+cal-M and Mod+cal-H received calycosin at daily doses of 5, 10, and 20 mg/kg [17], respectively. The treatment lasted for 14 consecutive days. Calycosin was dissolved in 0.5% carboxymethyl cellulose sodium (CMC-Na, S6703, Selleck, Shanghai, China) solution before administration. Meanwhile, the Con and Mod groups received the same volume of 0.5% CMC-Na via intragastric administration under the same procedure for 14 days.

Second, 36 SD rats were randomly assigned to six experimental groups via the random number table method, with six animals in each group: Con, Mod, Mod+ BAY11-7082, Mod+cal-H, Mod+cal-H+vector, and Mod+cal-H+NCOA2 groups. Rats in Con and Mod groups received the same treatments as those in the first batch. For the Mod+BAY11-7082 group, following 14 days of adenine administration, rats received intraperitoneal injection of the NF-κB inhibitor BAY11-7082 (HY-13453, MedChemExpress, NJ, USA) at a dosage of 5 mg/kg [18]. The treatment regimen consisted of one injection every three days, for a total of five administrations. BAY11-7082 was dissolved in dimethyl sulfoxide (DMSO, D274279, Aladdin-e, Shanghai, China) and further diluted with sterile saline before administration. For the Mod+cal-H group, following 14 days of adenine administration, rats received via oral gavage at a dose of 20 mg/kg once daily for a period of 14 consecutive

days. For the Mod+cal-H+vector and Mod+cal-H+NCOA2 groups, following 14 days of adenine administration, rats received calycosin orally at a dose of 20 mg/kg once daily for 14 days. Meanwhile, rats in the Mod+Cal-H+Vector and Mod+Cal-H+NCOA2 groups were intravenously injected via the tail vein with an equal volume of vehicle containing either the blank vector (negative control, pRP[Exp]-CMV, VectorBuilder, Suzhou, China) or the NCOA2 overexpression vector (pRP[Exp]-CMV>rNcoa2[NM_031822.3], VectorBuilder, Suzhou, China), respectively. Briefly, 10 μg of blank vector or NCOA2 overexpression vector was mixed with 15 μL of Lipofectamine 2000 (S30520, Shyuanye, Shanghai, China) and diluted with normal saline to a final volume of 250 μL before injection [19]. This dosing regimen was repeated every 5 days for a total of 3 administrations. Rats in the Con and Mod groups received the corresponding vehicle treatments, including 0.5% CMC-Na by oral gavage, DMSO/normal vehicle by intraperitoneal injection, and empty vector vehicle by tail vein injection, following the same administration schedule as the intervention groups.

The order of treatment administration and the timing of measurements for all animals were randomized, and the cage positions were assigned randomly throughout the experiment. To reduce potential bias, animal handling, drug administration, and outcome evaluation were performed in a blinded manner throughout the experimental period. Upon study termination, rats were deeply anesthetized with sodium pentobarbital (P3761, Sigma-Aldrich, St. Louis, MO, USA, 40 mg/kg body weight, i.p.), and blood samples were collected from the orbital sinus. Following blood collection, the rats were euthanized with an overdose of sodium pentobarbital (150 mg/kg, i.p.), and renal tissues were subsequently harvested for further analysis. Humane endpoints were defined prior to the study to minimize animal suffering. Animals were monitored daily for health status, and those exhibiting severe distress, weight loss exceeding 20%, or signs of moribundity were humanely euthanized to avoid unnecessary suffering.

Hematoxylin and Eosin (HE) and Masson's Trichrome Staining

The kidney tissues of rats were first fixed in 10% neutral formalin solution (MM1521, Maokangbio, Shanghai, China) for 24 hours, and then underwent alcohol (E111963, Aladdin-e, Shanghai, China) gradient dehydration, xylene (X112050, Aladdin-e, China) infiltration, and paraffin (MB4273-1, Meilunbio, Dalian, China) embedding. Next, tissue sections (4 μm) were prepared using a microtome (E0972, Beyotime, Shanghai, China) for subsequent histological staining. For HE staining, sections were first dewaxed in xylene and then rehydrated through a graded alcohol series. Subsequently, the sections were stained with hematoxylin solution for 5 min at room temperature following the standard protocol of the HE staining kit (C0105S, Beyotime, Shanghai, China). The stained sections were rinsed with running tap water, immersed in 1% hydrochloric acid alcohol for differentiation for 3–5 s, rinsed in water for 30 seconds, and then stained with eosin solution for 30 seconds. For Masson's trichrome staining, sections were dewaxed and rehydrated following the same procedure. Subsequent staining operations were strictly performed according to the instructions of the commercial Masson's trichrome staining kit (G1346, Solarbio, Beijing, China). All sections were finally dehydrated with graded ethanol, cleared with xylene, and mounted with neutral gum. After mounting, the stained tissue sections were observed under a CX33 microscope (×100, Olympus, Hachioji, Tokyo, Japan).

Semi-quantitative scoring of renal injury was performed based on HE and Masson's trichrome staining, following previously reported criteria [20,21]. Scoring was restricted to the renal cortex, and fields containing renal medulla, large blood vessels or tissue edges were excluded. Tubular injury and interstitial injury scores were evaluated using HE-stained sections. For tubular injury score: 0, no tubular atrophy or injury; 1, ≤25% of the cortical tubules exhibited atrophy or vacuolization accompanied by tubular epithelial shedding or necrosis; 2, 26%–50% of the cortical tubules exhibited atrophy or vacuolization accompanied by tubular epithelial shedding or necrosis; 3, >50% of the cortical tubules exhibited atrophy or vacuolization accompanied by tubular epithelial shedding or necrosis. For interstitial injury score: 0, no obvious lesions; 1, mild injury (<25% of cortical area involved); 2, moderate injury (25%–50% of cortical area involved); 3, severe injury (>50% of cortical area involved). Renal interstitial fibrosis was assessed by Masson's trichrome staining: 0, interstitial fibrosis occupying ≤5% of the cortical area; 1, mild fibrosis, interstitial fibrosis occupying 6%–25% of the cortical area; 2, moderate fibrosis, interstitial fibrosis occupying 26%–50% of the cortical area; 3, severe fibrosis, interstitial fibrosis occupying >50% of the cortical area. Ten non-overlapping random fields were captured from each kidney, and the mean score of the 10 fields was calculated for each individual animal. Three animals were analyzed per group. All scoring was performed by an observer blinded to group allocation. The results were presented as mean ± standard deviation (SD).

Enzyme-Linked Immunosorbent Assay (ELISA)

Rat blood samples were centrifuged to collect serum. The renal function biomarkers were detected using commercially available ELISA kits according to the manufacturer's protocols. Specifically, the levels of Scr (RX301343R, Ruixinbio, Quanzhou, China), BUN (YJ403798, Yuanjubio, China), uric acid (UA, CB10660-Ra, Coibo, Shanghai, China), interleukin-1 beta (IL-1β, E-EL-R0012, Elabscience, Wuhan, China), interleukin-6 (IL-6, ml107050, Mlbio, Shanghai, China), and tumor necrosis factor-alpha (TNF-α, ml002859, Mlbio, Shanghai, China)

were determined with the ELISA kits. All absorbance measurements were performed at 450 nm wavelength using a Synergy H1 microplate reader (BioTek, Winooski, VT, USA) for subsequent calculation and analysis.

Quantitative Real-Time Reverse Transcription Polymerase Chain Reaction (qRT-PCR)

Total RNA was isolated from freshly obtained rat kidney tissue using an RNA extraction kit (10606ES60, Yeasen, Shanghai, China). Thereafter, single-stranded complementary DNA (cDNA) was generated via reverse transcription using the AdvanceFast First Strand cDNA Synthesis Kit (11149ES10, Yeasen, Shanghai, China). For quantitative analysis, qRT-PCR was performed with specific primers and 2×Hieff PCR Master Mix (10102ES08, Yeasen, Shanghai, China) in a CFX96 Real-Time PCR Detection System (Bio-Rad, Hercules, CA, USA). The PCR protocol consisted of initial denaturation at 95 °C for 5 min, followed by 35 cycles of denaturation (95 °C, 30 s), annealing (60 °C, 30 s), and extension (72 °C, 30 s). Relative gene expression levels were calculated using the $2^{-\Delta\Delta Ct}$ method, with GAPDH as the internal control. The primer sequences (5′-3′) were: NCOA2 (forward: GGCAGCAGTTATTAACACGGG), (reverse: AGCTCTGCGAGTTCCTCTATG); NLRP3 (forward: GGTGACCTTGTGTGTGCTTG), (reverse: AGCTGAGCAAGCTAAAGGCT); GAPDH (forward: ACGGGAAACCCATCACCATC), (reverse: TCACAAACATGGGGGCATCA).

Western Blotting

Renal tissues were homogenized in radioimmunoprecipitation (RIPA) buffer (89900, Thermo Fisher Scientific, Waltham, MA, USA) to extract total proteins. Nuclear and cytoplasmic proteins were separately isolated with a nuclear and cytoplasmic protein extraction kit (PK10014, Proteintech, Rosemont, USA). All protein quantification was performed using the bicinchoninic acid assay (BCA) kit (23225, Pierce Biotechnology, Rockford, IL, USA). The quantified protein samples were then denatured and separated by 10% sodium dodecyl sulfate-polyacrylamide gel electrophoresis (SDS-PAGE, MP2019-1KIT, Maokangbio, Shanghai, China). Subsequently, the separated proteins were transferred onto polyvinylidene fluoride (PVDF) membranes (F619537-0001, Sangon Biotech, Shanghai, China) for further analysis. After blocking the membranes with 5% skim milk for one hour at room temperature, the protein samples were incubated overnight at 4 °C with a monoclonal antibody specific to NLRP3 (ab263899, 1/1000, 118 kDa, Abcam, Cambridge, UK), Cleaved GSDMD (33825-1-AP, 1/1000, 31kDa, Proteintech, Wuhan, China), gasdermin D (GSDMD, 1/1000, ab219800, 60 kDa, Abcam, Cambridge, UK), Cleaved Caspase-1 (#4199, 1/1000, 20kDa, CST, Danvers, USA), Caspase-1 (22915-1-AP, 1/1000, 45-47 kDa, 30 kDa, 35 kDa, Proteintech, Wuhan, China), phosphorylation (p)-NF-κB (ab76302, 1/1000, 65 kDa, Abcam, Cambridge, UK), NF-κB (ab16502, 0.5 µg/mL, 70 kDa, Abcam, Cambridge, UK), NCOA2 (ab10491, 1/1000, 159 kDa, Abcam, Cambridge, UK), LaminB1 (12987-1-AP, 1/1000, 66 kDa, Proteintech, Wuhan, China) and glyceraldehyde-3-phosphate dehydrogenase (GAPDH, ab9485, 1/2500, 37 kDa, Abcam, Cambridge, UK). Subsequently, the membranes were incubated with horseradish peroxidase (HRP)-conjugated secondary antibody (Goat Anti-Rabbit, ab97051, 1/5000, Abcam, Cambridge, UK) for 1 h at room temperature. Finally, the protein bands were visualized using enhanced chemiluminescence (ECL) reagents (KGC4603, KeyGene, Nanjing, China), and protein bands were visualized using a gel imaging system (Bio-Rad, Hercules, CA, USA). The gray intensity of protein bands was quantified using ImageJ software (Bethesda, MD, USA), with GAPDH serving as the internal reference. The ratios of cleaved GSDMD to total GSDMD, cleaved Caspase-1 to total Caspase-1, and p-NF-κB to total NF-κB were then calculated.

Molecular Docking Analysis

Molecular docking analysis was conducted to assess the potential interaction between calycosin and NCOA2. The three-dimensional (3D) structure of calycosin was obtained from the PubChem database with a CID of 5280448 (https://pubchem.ncbi.nlm.nih.gov/). The AlphaFold-predicted structure of NCOA2 (AF-Q15596-F1) was retrieved from the UniProt database (UniProt ID: Q15596). Protein–ligand preprocessing and visualization were performed using PyMOL (version 3.1.0a0), and geometric optimization of the ligand structure was carried out in Chem3D (version 22.0.0, 64-bit). PyMOL was used for the preprocessing of the NCOA2 protein to remove water molecules and extraneous ligands. The chemical structure of calycosin was energy-minimized using Chem3D, and then imported into PyMOL for docking preparation. Docking calculations were implemented with AutoDock Vina (version 1.1.2, The Scripps Research Institute, La Jolla, CA, USA). AutoDock Vina adopts a global optimization algorithm combining iterated local search and Monte Carlo simulation for conformational sampling. Its empirical scoring function evaluates receptor–ligand binding affinity by accounting for steric hindrance, hydrogen bonding, hydrophobic interactions and desolvation effects. The exhaustiveness parameter controls the thoroughness of the global search, and generated poses were sorted and clustered according to the predicted binding free energy. The docking grid box was centered at X: 6.34, Y: –0.95, Z: –0.63 with dimensions of 126 × 100 × 126 Å. Other key parameters were set as follows: exhaustiveness = 8 (default for Vina 1.1.2), num_modes = 20, energy_range = 3 kcal/mol (default for Vina 1.1.2), seed = –1979780192. The predicted binding affinity between the ligand and protein was evaluated based on binding energy (kcal/mol). For the interpretation of docking results, empirical binding energy thresh-

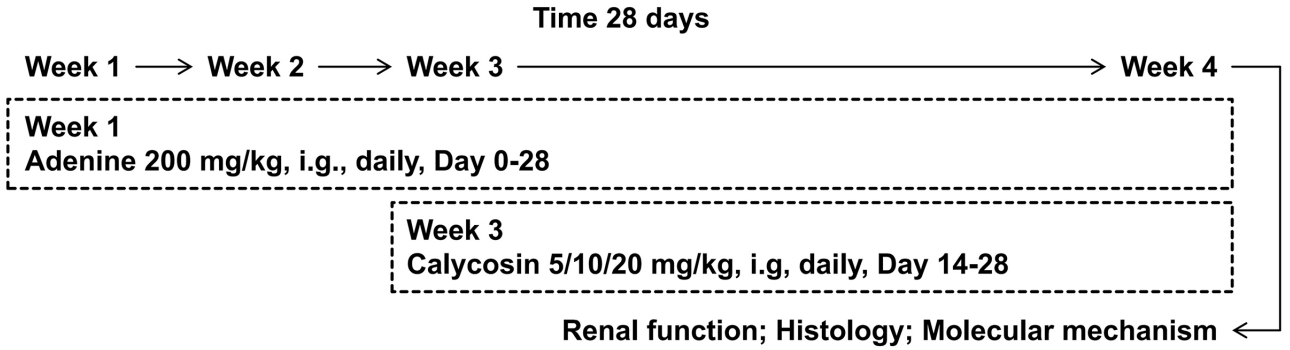


Fig. 1. Schematic timeline of CRF modeling and drug administration. CRF, chronic renal failure.

olds were applied: values <–4.25 kcal/mol indicate possible binding, values <–5.0 kcal/mol indicate favorable binding affinity, and values <–7.0 kcal/mol indicate high binding affinity from the simulation [22].

Terminal Transferase dUTP Nick End Labeling (TUNEL) Staining

Apoptosis was measured using the TUNEL kit (C1086, Beyotime, Shanghai, China). After the kidney tissue was fixed, embedded, sectioned, and dewaxed, 20 µg/mL proteinase K solution was added dropwise. After 30 minutes of incubation, 50 µL of TUNEL reaction solution was added to each sample. The samples were then incubated at 37 °C for an additional 60 minutes. Finally, nuclear counterstaining was performed using 4′,6-diamidino-2-phenylindole dihydrochloride (DAPI, C1002, Beyotime, Shanghai, China); sections were mounted and observed under fluorescence microscopy (DM750, ×200, Leica Microsystems, Wetzlar, Hesse, Germany), and positive signals were identified as green fluorescence.

Statistical Analysis

Statistical analyses were conducted using GraphPad Prism 8.0.2 software (Version 8.0.2, GraphPad Software, San Diego, CA, USA). Continuous variables are expressed as mean ± SD. Normality and homogeneity of variance tests were performed prior to statistical comparison. For multiple group comparisons, one-way analysis of variance (ANOVA) with Tukey's post hoc test was employed. Statistical significance was defined as $p < 0.05$.

Results

Calycosin Improved Renal Function and Suppressed NLRP3 in CRF Rat Models

To explore the renoprotective effects of calycosin in CRF, we established an adenine-induced CRF rat model and administered calycosin to the rats. Fig. 1 depicts the experimental schedule for rat modeling and treatment. Upon completion of the intervention, serum renal function markers were detected by ELISA. The results showed that the serum levels of Scr, BUN, and UA were significantly increased in the Mod group compared to the Con group (Fig. 2A–C, $p < 0.001$). In contrast, treatment with low-, medium-, or high-dose calycosin (Mod+cal-L, Mod+cal-M, and Mod+cal-H, respectively) markedly decreased levels of these parameters relative to the Mod group (Fig. 2A–C, $p < 0.01$). Compared with the control group, the kidney tissue in the model exhibited abnormal glomerular morphology, expanded tubular interstitium, marked interstitial injury, and prominent 2,8-dihydroxyadenine (2,8-DHA)-related crystal deposition in renal sections (Fig. 2D–F, $p < 0.001$). However, alleviation of these pathological injuries was observed in the calycosin-treated groups (Fig. 2D–F, $p < 0.01$). Furthermore, qRT-PCR and Western blot analyses demonstrated that NLRP3 expression was substantially upregulated in the Mod group compared to the Con group, while calycosin treatment at different concentrations dose-dependently suppressed NLRP3 expression (Fig. 2G–I, $p < 0.001$).

NCOA2 Overexpression Partially Reverses the Renoprotective Effects of Calycosin by Activating NF-κB Signaling in CRF Rats

Western blot assays were used to determine NCOA2 protein abundance in renal tissues from the Con, Mod and Mod+cal-H groups. The results demonstrated that NCOA2 expression was markedly upregulated in the Mod group, whereas calycosin-H treatment restored NCOA2 protein levels (Fig. 3A,B, $p < 0.05$). To further explore the potential interaction between calycosin and NCOA2, molecular docking simulations were conducted. These results indicated that calycosin may bind to NCOA2 with a favorable binding energy of –6.7 kcal/mol, representing a predicted favorable interaction. Further analysis revealed the formation of two hydrogen bonds between calycosin and NCOA2, supporting this predicted interaction (Fig. 3C). As shown in Fig. 2, high-dose calycosin exerted the most pronounced protective effect against renal injury and the strongest inhibitory effect on NLRP3 expression. Thus, this concentration was selected for subsequent NCOA2 rescue experiments. Compared with the Con group, NCOA2

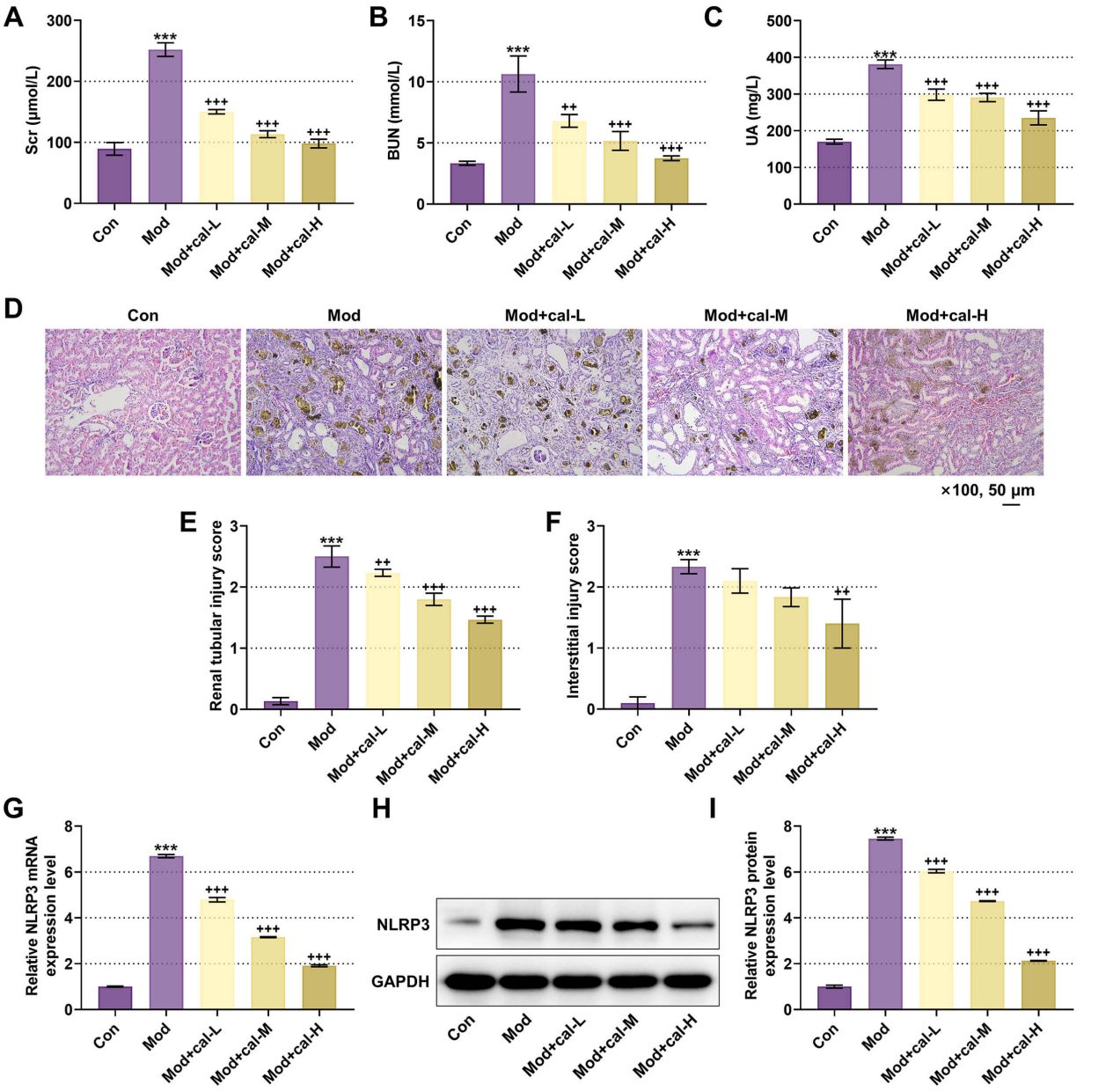


Fig. 2. Calycosin alleviated renal tissue injury, improved kidney function, and inhibited the activation of the NLR family pyrin domain-containing protein 3 (NLRP3) inflammasome in chronic renal failure (CRF) rat models. (A) The level of Serum creatinine (Scr) was determined by an enzyme-linked immunosorbent assay (ELISA) kit. (B) The level of blood urea nitrogen (BUN) was measured using an ELISA kit. (C) The level of uric acid (UA) was detected by an ELISA kit. (D) The pathological changes in renal tissues were detected by hematoxylin and eosin (HE) staining. Brown deposits represent 2,8-dihydroxyadenine (2,8-DHA)-related crystal deposition. Scale bar = 50 μm; magnification: ×100. (E,F) The score of renal tubular injury and renal interstitial injury. Ten non-overlapping random fields were captured per kidney, with three animals per group. (G) The mRNA expression of NLRP3 was measured by quantitative real-time polymerase chain reaction (qRT-PCR), with glyceraldehyde-3-phosphate dehydrogenase (GAPDH) serving as the internal reference gene. (H,I) The protein expression of NLRP3 was measured by Western blot assay, with GAPDH serving as the internal reference. $^{***}p < 0.001$ vs. Con; $^{++}p < 0.01$, $^{+++}p < 0.001$ vs. Mod. n = 6 independent biological replicates for panels (A–C) and n = 3 for panels (D–I). Data are presented as mean ± standard deviation.

mRNA and protein levels were significantly increased in the Mod group (Fig. 3D–F, $p < 0.001$). Notably, high-dose calycosin treatment (Mod+cal-H) markedly reduced NCOA2 expression relative to the Mod group; however, NCOA2 overexpression partially restored NCOA2 expression at both mRNA and protein levels (Fig. 3D–F, $p < 0.01$),

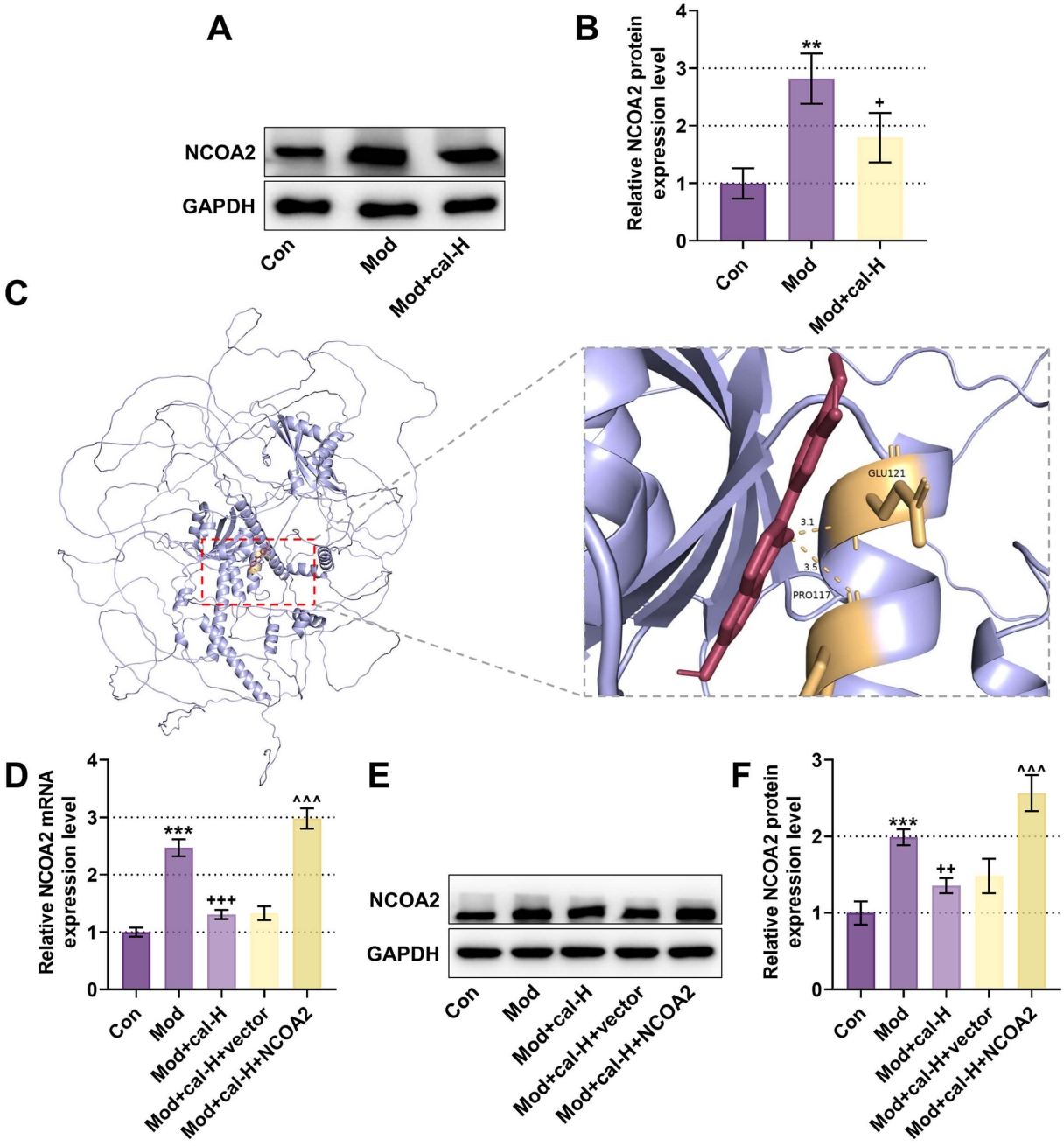


Fig. 3. Calycosin interacts with NCOA2 and modulates NCOA2 expression in adenine-induced CRF rats. (A,B) The protein expression of NCOA2 was measured by Western blotting in the Con, Mod and Mod+cal-H groups. (C) Molecular docking analysis revealed a predicted interaction between calycosin and NCOA2, with a binding energy of –6.7 kcal/mol. Calycosin is shown in red, and NCOA2 is shown in purple. Two hydrogen bonds were formed between calycosin and NCOA2 at residues GLU121 and PRO117. (D) The expression of NCOA2 was measured by qRT-PCR, with GAPDH serving as the internal reference gene. (E,F) The protein expression of NCOA2 was detected by Western blotting across all indicated groups. $^{**}p < 0.01$, $^{***}p < 0.001$ vs. Con; $^{+}p < 0.05$, $^{++}p < 0.01$, $^{+++}p < 0.001$ vs. Mod. $^{\wedge\wedge\wedge}p < 0.001$ vs. Mod+cal-H+vector. n = 3 independent biological replicates for panels (A,B) and (D–F). Data are presented as mean ± standard deviation.

confirming that plasmid delivery successfully upregulated NCOA2 and supporting the reliability of the *in vivo* overexpression model.

To investigate whether NCOA2 participates in calycosin-mediated regulation of NF-κB signaling during CRF progression, we performed a series of analyses. Biochemical assessments revealed that both the NF-κB inhibitor BAY11-7082 and high-dose calycosin significantly decreased the levels of Scr, BUN, UA, IL-1β, IL-6, and TNF-α compared with the Mod group (Fig. 4A–F,

$p < 0.01$). Notably, NCOA2 overexpression partially counteracted the renoprotective effects of high-dose calycosin (Fig. 4A–F, $p < 0.01$). Histopathological examination demonstrated that compared with the Mod group, BAY11-7082 and calycosin treatment effectively ameliorated kidney tissue damage, with reduced tubular injury and interstitial lesion scores (Fig. 4G–I, $p < 0.01$). However, NCOA2 overexpression partially abolished calycosin's therapeutic benefits, exacerbating renal damage (Fig. 4G–I, $p < 0.001$). Masson's trichrome staining and quantitative analysis further showed that BAY11-7082 and high-dose calycosin significantly reduced renal collagen deposition and interstitial fibrosis scores (Fig. 4J,K, $p < 0.001$). However, NCOA2 overexpression offset the protective effects of calycosin, aggravated renal pathological lesions, and increased fibrosis scores (Fig. 4J,K, $p < 0.001$). Molecular analyses showed that both BAY11-7082 and high-dose calycosin significantly suppressed NLRP3 mRNA levels, while NCOA2 overexpression partially reversed calycosin's inhibitory effects (Fig. 4L, $p < 0.001$).

TUNEL staining revealed few apoptotic cells, as indicated by weak green fluorescence, in the Con group, whereas extensive apoptosis, indicated by strong green fluorescence, was observed in the Mod group (Fig. 5A,B; $p < 0.001$). Both BAY11-7082 and calycosin treatment markedly reduced the number of apoptotic cells, as indicated by green fluorescence, though NCOA2 overexpression again partially attenuated calycosin's anti-apoptotic effects (Fig. 5A,B, $p < 0.05$). Western blot analysis demonstrated increased cleaved GSDMD/GSDMD, cleaved caspase-1/caspase-1, and p-NF-κB/NF-κB ratios in the Mod group (Fig. 5C–F, $p < 0.05$). These changes were attenuated upon BAY11-7082 and calycosin treatment (Fig. 5C–F, $p < 0.05$). Calycosin's suppression of these markers was partially reversed by NCOA2 overexpression (Fig. 5C–F, $p < 0.05$). We further performed nuclear-cytoplasmic fractionation followed by Western blotting to evaluate p65 nuclear translocation. Compared with the Con group, nuclear NF-κB p65 was elevated, and cytoplasmic NF-κB p65 was decreased in the Mod group (Fig. 6A–D, $p < 0.001$). BAY11-7082 and calycosin treatment reversed these changes (Fig. 6A–D, $p < 0.05$). However, NCOA2 overexpression partially abolished the suppressive effects of calycosin on NF-κB p65 nuclear translocation (Fig. 6A–D, $p < 0.05$).

Discussion

In the present study, we demonstrated that calycosin exerted renoprotective effects in CRF rats by improving renal function and alleviating renal histopathological alterations. Mechanistically, calycosin attenuated NF-κB signaling activation, inhibited NLRP3 inflammasome-associated inflammatory responses, and reduced pyroptosis-related molecular changes, including GSDMD expression. To the best of our knowledge, this study provides new evidence that calycosin protects against CRF progression, with its renoprotective effect associated with the NCOA2/NF-κB/NLRP3 axis.

The first important finding of this study is that calycosin exerted significant renoprotective effects by alleviating renal tissue injury and improving renal function in CRF rats. A previous study has demonstrated that calycosin protects against diabetic kidney disease by modulating ferroptosis-related pathways [23]. Moreover, calycosin alleviates acute kidney injury induced by ischemia-reperfusion, which is associated with its inhibition of macrophage migration inhibitory factor (MIF)-mediated inflammatory chemotaxis and suppression of NF-κB-mediated inflammation through the PPARγ/EGR1 pathway [24,25]. Consistent with these previous findings, our results show that calycosin significantly alleviated renal pathological alterations and reduced Scr, BUN, and UA in CRF rats. Notably, the renoprotective effects of calycosin were dose-dependent, indicating a potential dose-response relationship between calycosin administration and renal protection. Collectively, these findings provide experimental evidence supporting the therapeutic potential of calycosin for CRF treatment.

The core finding of this study is that calycosin exerts renoprotective effects in CRF primarily through the inhibition of NLRP3 inflammasome activation, which is associated with the NCOA2/NF-κB signaling axis. Increasing evidence indicates that excessive inflammasome activation plays a central role in renal inflammation and fibrosis, whereas inhibition of inflammasome-related pathways effectively alleviates renal injury [26]. Moreover, NLRP3 has been proposed as a potential biomarker for evaluating therapeutic responses and predicting prognosis in CRF patients undergoing hemodialysis [27]. Pyroptosis, a form of programmed inflammatory cell death, plays a context-dependent role in renal homeostasis. While moderate levels of pyroptosis contribute to physiological regulation, excessive pyroptotic activation leads to the uncontrolled release of pro-inflammatory mediators and exacerbates tissue damage [28,29]. In line with this notion, recent investigations have demonstrated that Bushen Huoxue formula attenuates renal fibrosis and pyroptosis in chronic kidney disease by inhibiting ROS/NLRP3-mediated inflammasome activation [30]. In agreement with previous findings [31,32], our results demonstrate that calycosin significantly suppressed NLRP3 expression and downstream inflammatory responses, accompanied by decreased ratios of cleaved GSDMD/GSDMD and cleaved caspase-1/caspase-1, as well as reduced p-NF-κB/NF-κB, suggesting that inhibition of NLRP3 inflammasome activation and modulation of pyroptosis-related molecular mechanisms contribute to its renoprotective effects.

Since NF-κB signaling serves as a critical upstream regulator of NLRP3 activation, we further investigated the

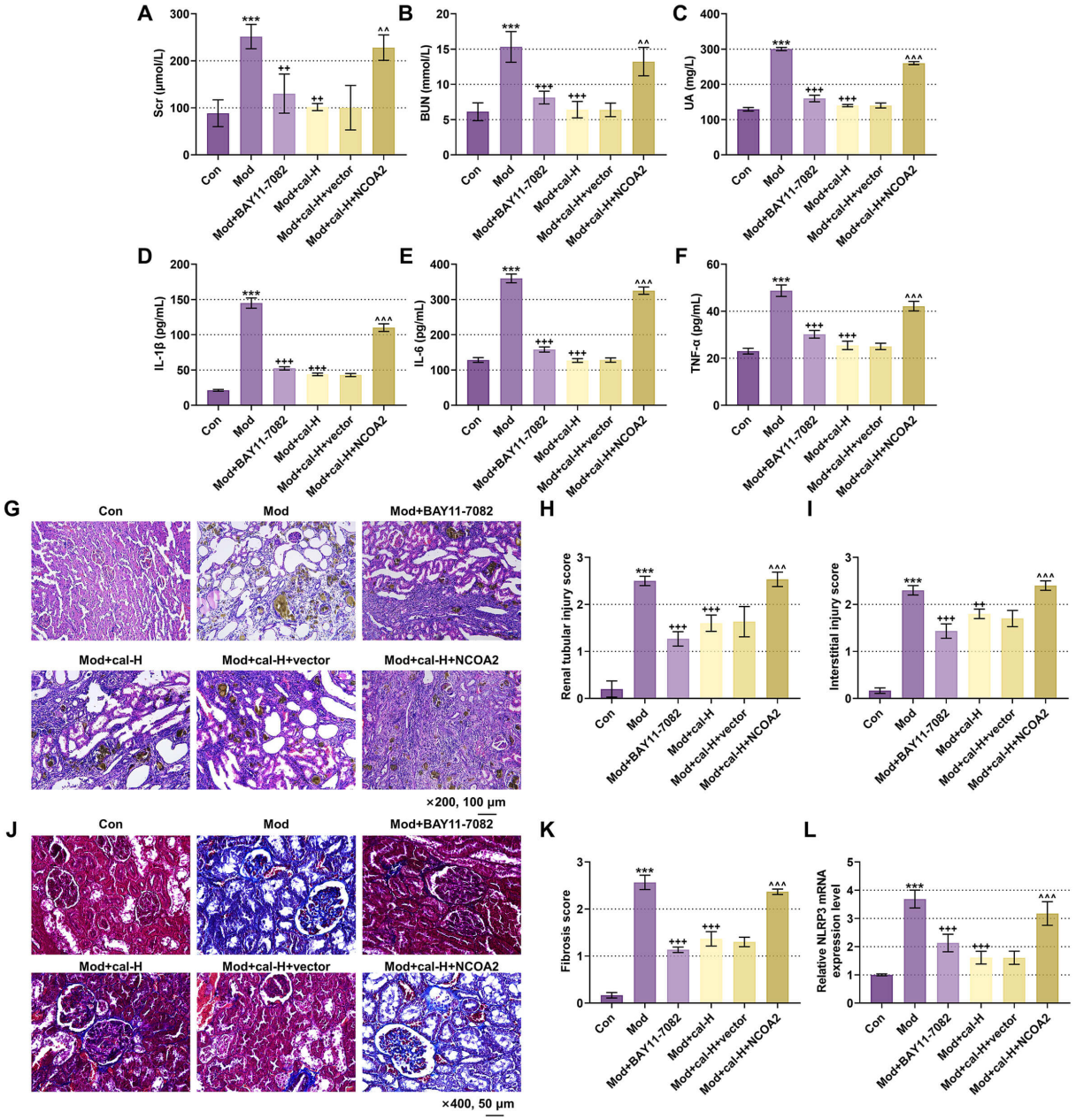


Fig. 4. The overexpression of NCOA2 partially reverses the beneficial effects of calycosin on tissue damage and kidney function. (A–F) The levels of Scr, BUN, UA, interleukin-1 beta (IL-1β), interleukin-6 (IL-6), and tumor necrosis factor-alpha (TNF-α) were assessed using an ELISA kit. (G) The pathological changes in renal tissues were detected by HE staining. Brown deposits represent 2,8-DHA-related crystal deposition. Scale bar = 100 μm; magnification: ×200. (H,I) The score of renal tubular injury and renal interstitial injury. Ten non-overlapping random fields were captured per kidney, with three animals per group. (J) Masson's trichrome staining was performed to evaluate renal interstitial fibrosis. Bar = 50 μm; magnification: ×400. (K) The score of renal interstitial fibrosis. Ten non-overlapping random fields were captured per kidney, with three animals per group. (L) The level of NLRP3 was measured by qRT-PCR, with GAPDH serving as the internal reference gene. $^{***}p < 0.001$ vs. Con; $^{++}p < 0.01$, $^{+++}p < 0.001$ vs. Mod. $^{\wedge\wedge}p < 0.01$, $^{\wedge\wedge\wedge}p < 0.001$ vs. Mod+cal-H+vector. n = 6 independent biological replicates for panels (A–F), and n = 3 for panels (G–L). Data are presented as mean ± standard deviation.

mechanisms underlying the anti-inflammatory actions of calycosin. The NLRP3 inflammasome can further amplify NF-κB-driven inflammatory signaling through the maturation and release of IL-1β, creating a positive feedback loop that promotes persistent renal inflammation [12]. Previous studies have demonstrated that targeting the NF-κB pathway improves renal function and attenuates inflammatory injury in CRF models [33,34]. Importantly, our bioin-

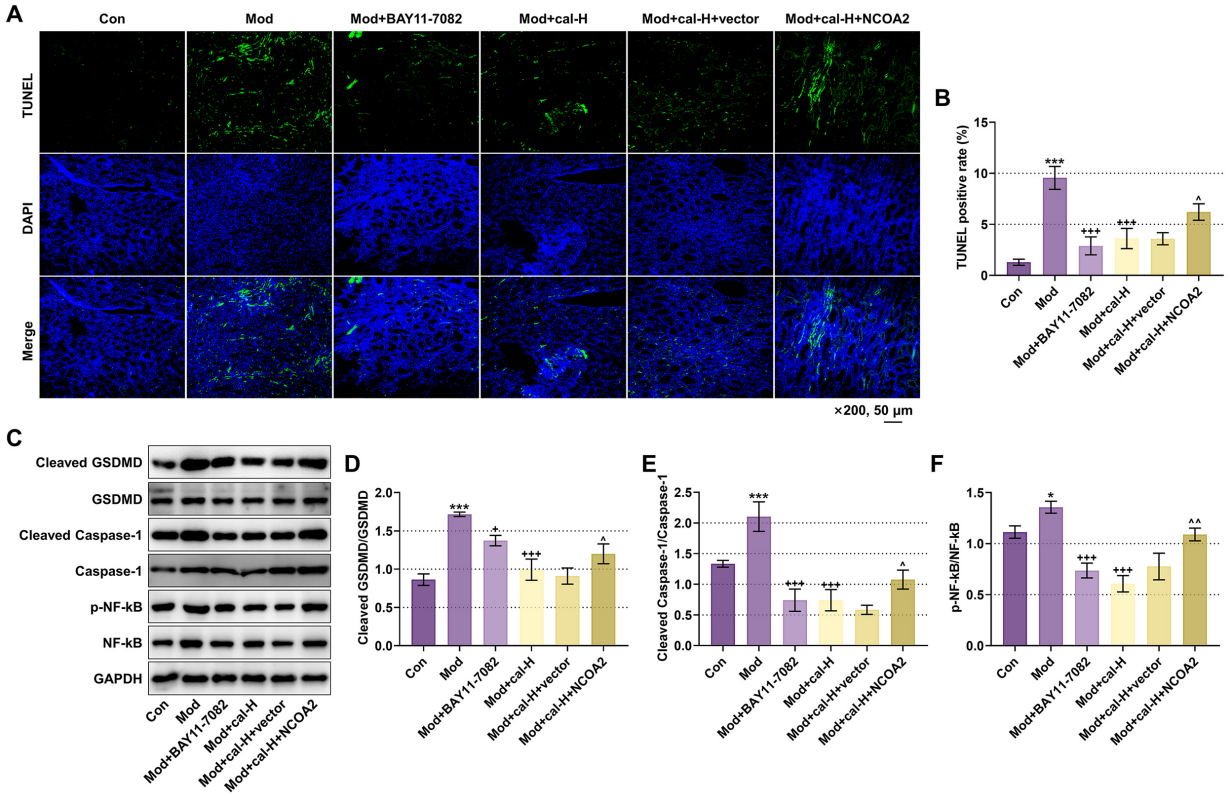


Fig. 5. The overexpression of NCOA2 partially reverses the inhibitory effects of calycosin on apoptosis and pyroptosis-related and nuclear factor kappa-B (NF-κB) proteins. (A,B) Representative TUNEL staining images (A) and quantification of TUNEL positive rate (B). Scale bar = 50 μm; magnification: ×200. TUNEL positive apoptotic cells were visualized by green fluorescence. (C–F) Representative Western blot images and quantitative analysis of the ratios of Cleaved gasdermin D (GSDMD)/GSDMD, Cleaved Caspase-1/Caspase-1 and phosphorylated NF-κB (p-NF-κB)/NF-κB. GAPDH served as the internal reference. $^{*}p < 0.05$, $^{***}p < 0.001$ vs. Con; $^{+}p < 0.05$, $^{+++}p < 0.001$ vs. Mod. $^{\wedge}p < 0.05$, $^{\wedge\wedge}p < 0.01$ vs. Mod+cal-H+vector. n = 3 independent biological replicates for panels (A–F). Data are presented as mean ± standard deviation.

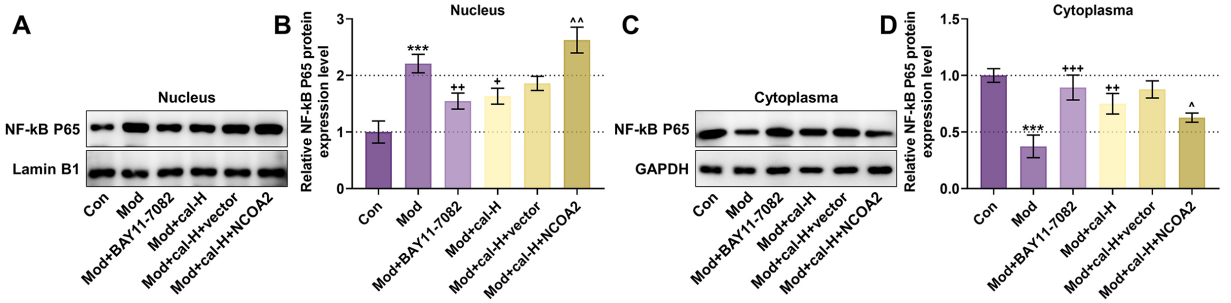


Fig. 6. NCOA2 overexpression partially reverses calycosin-mediated inhibition of NF-κB p65 nuclear translocation. (A,B) The levels of nuclear NF-κB p65 were assessed by Western blotting after nuclear-cytoplasmic fractionation, and Lamin B1 was used as the internal reference for nuclear protein. (C,D) The levels of cytoplasmic NF-κB p65 were assessed by Western blotting after nuclear-cytoplasmic fractionation, and GAPDH was used as the internal reference for cytoplasmic protein. $^{***}p < 0.001$ vs. Con; $^{+}p < 0.05$, $^{++}p < 0.01$, $^{+++}p < 0.001$ vs. Mod. $^{\wedge}p < 0.05$, $^{\wedge\wedge}p < 0.01$ vs. Mod+cal-H+vector. n = 3 independent biological replicates for panels (A–D). Data are presented as mean ± standard deviation.

formatics analysis and molecular docking results predicted NCOA2 as a potential target for calycosin. In the present study, both the NF-κB inhibitor BAY11-7082 and calycosin treatment markedly suppressed NF-κB p65 nuclear translocation, reduced inflammatory factor production and ameliorated renal injury. Notably, overexpression of NCOA2 partially reversed the inhibitory effects of calycosin on NF-κB/NLRP3 activation and inflammatory responses, indicat-

ing that NCOA2 may act as a critical mediator for the anti-inflammatory effects of calycosin in this adenine-induced CRF rat model. Collectively, these findings indicate that calycosin protects against CRF progression by modulating the NCOA2/NF-κB signaling pathway, thereby suppressing NLRP3 inflammasome activation and inflammatory responses, alongside modulation of pyroptosis-related molecular mechanisms. This study provides new mechanistic insights into the renoprotective effects of calycosin and suggests that NCOA2 may serve as a potential therapeutic target in the treatment of CRF.

However, the study still has limitations. First, although our findings suggest that calycosin regulates the NCOA2/NF-κB/NLRP3 axis, the interaction between calycosin and NCOA2 is only supported by bioinformatics predictions and molecular docking analyses. Notably, the molecular docking analysis was performed using the human NCOA2 structure, whereas our *in vivo* experiments were conducted in rats. Therefore, this predicted binding interaction requires further experimental validation. Second, additional NCOA2 loss-of-function studies are needed to further establish its essential role in calycosin-mediated renoprotection. Moreover, it should be noted that our non-targeted *in vivo* plasmid delivery strategy could not identify the specific renal cell types where NCOA2 was overexpressed. Future cell-type-specific investigations are required to clarify whether the function of NCOA2 is cell-type dependent. Finally, the efficacy and safety of calycosin in humans require further clinical evaluation before clinical translation.

Conclusion

This study suggests that calycosin may alleviate renal injury in CRF by regulating the NCOA2/NF-κB/NLRP3 signaling axis, which suppresses inflammatory responses and modulates pyroptosis-related molecular mechanisms. These findings offer new insights into the molecular mechanisms underlying the renoprotective effects of calycosin and support its potential renal protective effect of CRF. However, further preclinical studies are required to explore its potential for CRF intervention.

Availability of Data and Materials

The analyzed datasets generated during the study are available from the corresponding author on reasonable request.

Author Contributions

JGY and WZY designed the research study; XYZ and SBL performed the research; HZM and LL collected and analyzed the data. LL has been involved in drafting the manuscript, and all authors have been involved in revising it critically for important intellectual content. All authors gave final approval of the version to be published. All authors have participated sufficiently in the work to take public responsibility for appropriate portions of the content and agreed to be accountable for all aspects of the work in ensuring that questions related to its accuracy or integrity are appropriately investigated and resolved.

Ethics Approval and Consent to Participate

All animal experimental procedures in this study were approved by the Animal Ethics Committee of the Zhejiang Provincial Animal Center (Approval No. ZJCLA-IACUC-20110060). All animal studies were conducted and reported in strict accordance with the ARRIVE 2.0 guidelines.

Acknowledgment

Not applicable.

Funding

This work was supported by The Zhejiang Provincial Traditional Chinese Medicine Science and Technology Plan Project (grant number: 2024ZL793).

Conflict of Interest

The authors declare no conflict of interest.

References

[1] Temirovich AM, Ugli KYE, Akbarjon F, Khumoyun B. CRF AND CKD: MODERN APPROACHES TO TERMINOLOGY, CLASSIFICATION, DIAGNOSIS AND TREATMENT. Research Focus International Scientific Journal. 2023; 2: 79–90. https://doi.org/10.66073/researchfocus.v2i1.2827

[2] Liu W, Hu C, Qian X, He C, Gu R, Meng Z, et al. Tao-HeChengQi Decotion alleviate chronic renal failure via regulation of PHD2/UCP1 and RIPK3/AKT/TGF-β pathway. Phytomedicine: International Journal of Phytotherapy and Phytopharmacology. 2025; 141: 156548. https://doi.org/10.1016/j.phymed.2025.156548

[3] Herrington WG, Judge PK, Grams ME, Wanner C. Chronic kidney disease. Lancet (London, England). 2026; 407: 90–104. https://doi.org/10.1016/S0140-6736(25)01942-7

[4] Johansen KL, Chertow GM, Gilbertson DT, Ishani A, Israni A, Ku E, et al. US Renal Data System 2022 Annual Data Report: Epidemiology of Kidney Disease in the United States. American Journal of Kidney Diseases: the Official Journal of the National Kidney Foundation. 2023; 81: A8–A11. https://doi.org/10.1053/j.ajkd.2022.12.001

[5] Yazgan B, Avcı F, Memi G, Tastekin E. Inflammatory response and matrix metalloproteinases in chronic kidney failure: Modulation by adropin and spexin. Experimental Biology and Medicine (Maywood, N.J.). 2021; 246: 1917–1927. https://doi.org/10.1177/15353702211012417

[6] Huang G, Zhang Y, Zhang Y, Ma Y. Chronic kidney disease and NLRP3 inflammasome: Pathogenesis, development and targeted therapeutic strategies. Biochemistry and Biophysics Reports. 2023; 33: 101417. https://doi.org/10.1016/j.bbrep.2022.101417

[7] Sabra MS, Hemida FK, Allam EAH. Adenine model of chronic renal failure in rats to determine whether MCC950, an NLRP3 inflammasome inhibitor, is a renopreventive. BMC Nephrology. 2023; 24: 377. https://doi.org/10.1186/s12882-023-03427-4

[8] Hou Y, Lin S, Qiu J, Sun W, Dong M, Xiang Y, et al. NLRP3 inflammasome negatively regulates podocyte autophagy in diabetic nephropathy. Biochemical and Biophysical Research Communications. 2020; 521: 791–798. https://doi.org/10.1016/j.bbrc.2019.10.194

[9] Gao X, Chen L, Zhang C, Gao H, Yang S, Huang G, et al. Total Panax notoginseng saponins treats diabetic kidney disease in mice by regulating the TXNIP/NLRP3 signaling pathway. Clinical Traditional Medicine and Pharmacology. 2025; 6: 200245. https://doi.org/10.1016/j.ctmp.2025.200245

[10] Lu L, Rui Q, Yupeng C, Qing N. Investigating the application value of Shenqi Pill in cardiovascular-renal-metabolic syndrome based on hemodynamics. Chinese Journal of Basic Traditional Chinese Medicine. 2025; 31: 2032–2037. (In Chinese)

[11] Fang H, Zhou L, Xu X, Zhang T, Li S, Jin C. Angelicin Mitigating Renal Fibrosis and Treating IgA Nephropathy via the ESR1-FOS Pathway. Discovery Medicine. 2025; 37: 2214–2223. https://doi.org/10.24976/Discov.Med.202537201.188

[12] Dalal D, Singh L, Singh A. Calycosin and kidney health: a molecular perspective on its protective mechanisms. Pharmacological Reports: PR. 2025; 77: 658–669. https://doi.org/10.1007/s43440-025-00728-3

[13] Cao W, Huang L, Yu H, Qian Y, Liu L, Xu M, et al. Calycosin extracted from Astragali Radix reduces NETs formation to improve renal fibrosis via TLR4/NF-κB pathway. Journal of Ethnopharmacology. 2025; 342: 119391. https://doi.org/10.1016/j.jep.2025.119391

[14] Wang Y, Bai X, Pei R, Lei W, Zhang Z, Dai P. Calycosin Attenuates Endoplasmic Reticulum Stress Injury in Human Renal Glomerular Endothelial Cells by Inhibiting SRC/SYKDependent Reactive Oxygen Species. Current Molecular Medicine. 2026. https://doi.org/10.2174/0115665240473729260504092344 (online ahead of print)

[15] Zhou P, Li D, Luo F, Wan X. NCOA2 coordinates with the transcriptional KAT2B-NF-κB partner to trigger inflammation response in acute kidney injury. Gene. 2022; 832: 146583. https://doi.org/10.1016/j.gene.2022.146583

[16] Zhou J, Zhou H, Liu C, Huang L, Lu D, Gao C. HDAC1-mediated deacetylation of LSD1 regulates vascular calcification by promoting autophagy in chronic renal failure. Journal of Cellular and Molecular Medicine. 2020; 24: 8636–8649. https://doi.org/10.1111/jcmm.15494

[17] Yang X, Pan Y, Cai L, Wang W, Zhai X, Zhang Y, et al. Calycosin Ameliorates Neuroinflammation via TLR4-Mediated Signal Following Cerebral Ischemia/Reperfusion Injury in vivo and in vitro. Journal of Inflammation Research. 2024; 17: 10711–10727. https://doi.org/10.2147/JIR.S480262

[18] Bi R, Chen K, Wang Y, Luo X, Li Q, Li P, et al. Regulating Fibrocartilage Stem Cells via TNF-α/Nf-κB in TMJ Osteoarthritis. Journal of Dental Research. 2022; 101: 312–322. https://doi.org/10.1177/00220345211037248

[19] Wei L, Zhang X, Ye Q, Yang Y, Chen X. The transfection of A20 gene prevents kidney from ischemia reperfusion injury in rats. Molecular Medicine Reports. 2017; 16: 1486–1492. https://doi.org/10.3892/mmr.2017.6725

[20] Qiao Y, Sun C, Kan S, He L, Wang Y, Gao H, et al. SRS 16-86 promotes diabetic nephropathy recovery by regulating ferroptosis. Experimental Physiology. 2024; 109: 1199–1210. https://doi.org/10.1113/EP091520

[21] Honetschlägerová Z, Sadowski J, Kompanowska-Jezierska E, Maxová H, Táborský M, Kujal P, et al. Impaired renal autoregulation and pressure-natriuresis: any role in the development of heart failure in normotensive and angiotensin II-dependent hypertensive rats? Hypertension Research: Official Journal of the Japanese Society of Hypertension. 2023; 46: 2340–2355. https://doi.org/10.1038/s41440-023-01401-z

[22] Li C, Shi Y, Zuo L, Xin M, Guo X, Sun J, et al. Identification of Biomarkers Associated with Cancerous Change in Oral Leukoplakia Based on Integrated Transcriptome Analysis. Journal of Oncology. 2022; 2022: 4599305. https://doi.org/10.1155/2022/4599305

[23] Huang D, Shen P, Wang C, Gao J, Ye C, Wu F. Calycosin plays a protective role in diabetic kidney disease through the regulation of ferroptosis. Pharmaceutical Biology. 2022; 60: 990–996. https://doi.org/10.1080/13880209.2022.2067572

[24] Wang HL, Peng Z, Li YQ, Wang YX, Li JC, Tan RZ, et al. Calycosin inhibited MIF-mediated inflammatory chemotaxis of macrophages to ameliorate ischemia reperfusion-induced acute kidney injury. Inflammation Research. 2024; 73: 1267–1282. https://doi.org/10.1007/s00011-024-01899-0

[25] Zhang N, Guan C, Liu Z, Li C, Yang C, Xu L, et al. Calycosin attenuates renal ischemia/reperfusion injury by suppressing NF-κB mediated inflammation via PPARγ/EGR1 pathway. Frontiers in Pharmacology. 2022; 13: 970616. https://doi.org/10.3389/fphar.2022.970616

[26] Islamuddin M, Qin X. Renal macrophages and NLRP3 inflammasomes in kidney diseases and therapeutics. Cell Death Discovery. 2024; 10: 229. https://doi.org/10.1038/s41420-024-01996-3

[27] Huang X, Wang S, Yan K, Liu C, Zhang Q, Wu N. Assessment of HMGB1 and NLRP3 in Determining Efficacy and Prognosis in Hemodialysis Patients with Chronic Renal Failure. Alternative Therapies in Health and Medicine. 2024; 30: 478–482.

[28] Zhu Y, Huang G, Yang Y, Yong C, Yu X, Wang G, et al. Chinese Herbal Medicine Suyin Detoxification Granule Inhibits Pyroptosis and Epithelial-Mesenchymal Transition by Downregulating MAVS/NLRP3 to Alleviate Renal Injury. Journal of Inflammation Research. 2021; 14: 6601–6618. https://doi.org/10.2147/JIR.S341598

[29] Yu R, Wang X, Chen T, Xu J. Histone Lactylation Promotes Transcriptional Activation of YTHDF2 in High Glucose-Induced Renal Injury by Enhancing m6A Modification of GDF15. Discovery Medicine. 2025; 37: 2411–2427. https://doi.org/10.24976/Discov.Med.202537201.204

[30] Liao L, Tao P, Xu Q, Chen J, Liu W, Hu J, et al. Bushen Huoxue formula protects against renal fibrosis and pyroptosis in chronic kidney disease by inhibiting ROS/NLRP3-mediated inflammasome activation. Renal Failure. 2024; 46: 2354444. https://doi.org/10.1080/0886022X.2024.2354444

[31] Yosri H, El-Kashef DH, El-Sherbiny M, Said E, Salem HA. Calycosin modulates NLRP3 and TXNIP-mediated pyroptotic signaling and attenuates diabetic nephropathy progression in diabetic rats; An insight. Biomedicine & Pharmacotherapy = Biomedecine & Pharmacotherapie. 2022; 155: 113758. https://doi.org/10.1016/j.biopha.2022.113758

[32] Pan Y, Nie L, Chen W, Guan D, Li Y, Yang C, et al. Buyang Huanwu Decoction prevents hemorrhagic transformation after delayed t-PA infusion via inhibiting NLRP3 inflammasome/pyroptosis associated with microglial PGC-1α. Journal of Ethnopharmacology. 2025; 340: 119275. https://doi.org/10.1016/j.jep.2024.119275

[33] Zhong G, Cai X, Wei R, Wei S, Cao X. Curcumenol improves renal function in 5/6 nephrectomy-induced chronic renal failure rats via the SIRT1/NF-κB pathway. Anatomical Record (Hoboken, N.J.: 2007). 2023; 306: 3189–3198. https://doi.org/10.1002/ar.25137

[34] Luo H, Wang M, Xu K, Peng Q, Zou B, Yin S, et al. Effect of Fushengong Decoction on PTEN/PI3K/AKT/NF-κB Pathway in Rats With Chronic Renal Failure via Dual-Dimension Network Pharmacology Strategy. Frontiers in Pharmacology. 2022; 13: 807651. https://doi.org/10.3389/fphar.2022.807651